TECHNICAL ARTICLE

Effect of Filler Wire on Laser Lap Welding of Al-Si Coated 22MnB5 Hot Stamping Steel

Feng Zhao, Youqiong Qin, Danfeng Zhang, and Min Liang

To suppress the accumulation of δ-ferrite and adjust the dilution of the Al-Si coating, 22MnB5 coated with Al-Si was laser lap welded with filler wire. The weld appearance, dilution of the coating, microstructure, and mechanical properties of the joints were studied. A mathematical model was established by energy conservation between the feeding speed and weld appearance and between the feeding speed and dilution of the base material. When the feeding speed was raised, the weld gradually changed from a tall cup shape to a bowl shape and the dilution of the coating decreased. This led to the reduction of the δ-ferrite. The fusion zone (FZ) was lath-like martensite (M). Four zones along the FZ to base material (BM) were formed in HAZ. The coarse grain heat-affected zone (CGHAZ) near FZ and the fine grain heat-affected zone (FGHAZ) consisted of martensite. The intercritical heat-affected zone (ICGHAZ) near BM consisted of martensite and a small amount of ferrite. The tempered zone (TZ) consisted of tempered martensite with the lowest hardness. Importantly, band-like (δ-ferrite) which had low strength and ductility occurred along the fusion boundary and became a weak region. The ultimate tensile strength was only 436 MPa without filler wire but reached 746 MPa with filler wire whose failure mode mixed dimpled and quasi-cleavage fracture.

1. Introduction

The lightweight concept promoted the development of ultrahigh-strength steels (UHSS) in the automotive industry. Some components, for example A, B, and C pillars and door beams, have been made up of UHSS (Ref 1-3). 22MnB5 hot stamping steel is a microalloyed boron steel, and its ultimate tensile strength can exceed 1.5 GPa through full martensite transformation after hot stamping. During the process, steel with alloyed boron is heated up above 900 °C for several minutes in a furnace, then compressed and then quenched in a closed die at a cooling rate of over 30 °C/s (Ref 4). However, to solve some problems, such as strong high-temperature oxidation and decarburization, various types of coating systems have been applied to the surface (Ref 5). 20-40 μm of Al-Si is commonly used as the coating on the surface that possesses excellent high-temperature oxidation resistance (Ref 6).

With the characteristics of precise energy control, fast processing speeds, small deformation, and high welding quality, laser welding was effectively used to join 22MnB5 with Al-Si. In the research, many problems also existed in laser welding 22MnB5 with Al-Si (Ref 7-10).

One problem of laser welding of hot stamping steels is HAZ softening because of the tempering of martensite. Jia et al. (Ref 11) studied the butt welding of 22MnB5. The fracture occurred in HAZ where the microhardness was only 300 HV. The microstructure of the softened zone was tempered martensite. Our previous research also reported that the lowest hardness was found in the outer-HAZ (Ref 12). To increase the hardness of HAZ, Gerhards et al. (Ref 13) welded the specimens in devices at − 98 °C and − 70 °C that were cooled in a mixing gas with liquid nitrogen and gaseous nitrogen, but the strength of the joint was not dramatically increased.

Another problem is the gathering of the Al-Si coating at FB. After coating Al-Si on the hot stamping steel, the fracture often occurs in the FB but not in the softening HAZ zone (Ref 14). Kang et al. (Ref 15) reported that the Al-Si coating melted and moved into the pool. The rich-Al structure was formed at FB and possessed low ductility and strength. The welded joint with Al-Si coating had low strength and fractured at the FZ, but the welded joint without Al-Si coating had high strength and fractured in the HAZ. Kim et al. (Ref 16) considered the Al-rich phase as Fe-Al brittle intermetallic (IMC), but many other researchers disagreed with it, such as Lin et al. (Ref 17), Saha et al. (Ref 18), considering it was δ-ferrite because Al is a strong ferrite stabilizer (Ref 19, 20) and Al content at the FB is not so high to form a compound (IMC compound at least needs 12 wt.% Al). Moreover, many researchers have tried to find some methods to alleviate the influence of Al-Si. Some researchers removed the coating before welding by laser cleaning, shotblasting, or sanding. For example, Flehmig

Feng Zhao, Danfeng Zhang, and Min Liang, School of Material Engineering, Shanghai University of Engineering Science, Shanghai 201620, People's Republic of China; and Youqiong Qin, School of Material Engineering, Shanghai University of Engineering Science, Shanghai 201620, People's Republic of China; and Shanghai Collaborative Innovation Center of Laser Advanced Manufacturing Technology, Shanghai University of Engineering Science, Shanghai 201620, People's Republic of China. Contact e-mail: qyqqin@163.com.

et al. (Ref 21) patented mechanical grinding to clean Al-Si, for example, tools combined with a press and scraper, or a scraper roller. Min et al. (Ref 22) reported the strength raised by the laser cleaning and sanding. Other researchers modified the welding parameters to increase the strength. Kügler et al. (Ref 23) found that by increasing the spot size or the parallel weld path, the weld width of the joint increased and the dispersal of the Al-rich phase at FZ improved. Accordingly, the strength increased. Qin et al. (Ref 12, 24) studied the changes in the microscopic structure and properties of lap joints by varying welding parameters and found that although the tensile shear strength with the coating was lower than that of the joint without coating, the strength improved with raising the laser power or reducing the welding speed, probably owing to the enhanced convection in the melt pool with high heat input.

From the above studies, rich-Al coating is an important factor in deteriorating the strength of laser welding 22MnB5. As we know, filler wire is often added as a dilution material to the weld to modify the microscopic structure and increase the strength. Lin et al. (Ref 25) found that in laser butt welding the Al-Si coated 22MnB5, a carbon steel filler wire was applied to dilute Al. The amount of δ-ferrite decreased due to dilution and homogenization of Al. However, the influence of filler wire on the characteristics of joints needs to be deeply discussed, especially the lap joint. Moreover, mathematical model can be used to easily understand the welding appearance and the relationship between the dilution and the welding parameter. In this study, laser lap welding of Al-Si coated 22MnB5 was experimented with different feeding speeds. The dilution process was studied. The appearance, microstructure and mechanical properties of the welded joints were also discussed.

2. Experimental Procedures

For this experiment, 1 mm thick Al-Si coated 22MnB5 hot stamping steel and a 1.2 mm diameter filler wire were adopted. Approximately 30 μm of Al-Si was coated on both sides. The 22MnB5 steel was austenitized in a furnace at 900 °C for 5 min and then press-hardened (at an approximate average cooling rate of 30 °C/s) between two flat dies. The microstructure of the base material and the coating is shown in Fig. 1. The base material had a fully martensitic microstructure. The chemical compositions of the coating are shown in Table 1. The Al-Si

coating consisted of three regions: I, II, and III, as shown in Fig. 1(a). Region I was close to the base metal, and its main composition was Fe. The phase in region I was probably α-Fe(Al, Si). In the regions II and III, the atomic ratios of Fe to Al and Si were about 2:5 and 1:1, which means the phases were probably Fe2(Al,Si)5 and Fe(Al,Si), respectively. The microstructure result was the same as our previous research of Al-Si coated 22MnB5 with 30 μm (Ref 12, 24). The chemical compositions (wt.%) and the tensile properties are shown in Table 2. The ultimate tensile strength (UTS), the yield strength (YS) and the elongation of 22MnB5 were about 1500 MPa, 1200 MPa and 4.1%, respectively. 22MnB5 sheets were cut into 100 mm 80 mm 1 mm sheets for the experiment.

The IPG YLS-5000 laser installed on the KUKA robot was used for laser lap welding with filler wire. The laser wavelength is 1060-1080 nm. The focal distance is 310 mm. The diameter of the laser spot is 0.4 mm. The welding speed and welding power are fixed at 2 m/min and 2.5 kW, respectively. A schematic of laser lap welding added by filler wire is given in Fig. 2. The defocus amount is fixed at + 3 mm. laser beam perpendicularly devoted to the 22MnB5 upper surface. To improve, the feeding angle α of filler wire is 45°. In the feeding stability, filler wire was put in a Cu tube. A laser beam was placed behind the filler wire. The shielding gas was pure argon gas (99.99%) with a flow rate of 15 L/min. Table 3 gives the welding parameters for this experiment. To contrast the differences in joints' microstructural transformation and mechanical properties, the variable feeding speed of filler wire (parameter No. 1/2/3/4) was chosen. All the specimens were degreased with acetone before welding.

The specimens cut perpendicularly to the weld were used for tension shear testing and metallography observing. Fig. 3 gives the dimensions of the mechanical test specimen. Tension shear

Table 1 Chemical compositions (at.%) of the marked phases in Fig. 1(b)

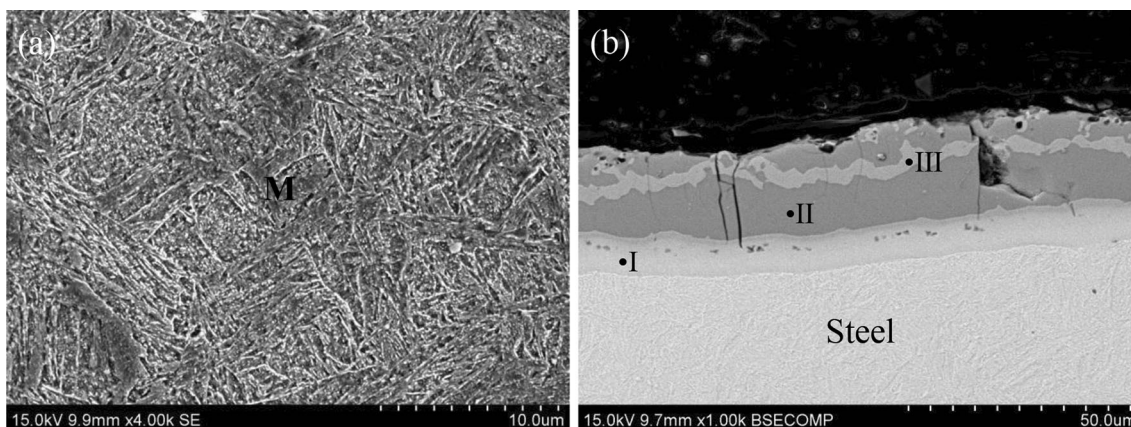|	Chemical compositions (at.%)				Probable phases
	Al	**Si**	**Zn**	**Fe**	
I	14.57	4.82	…	Bal.	α-Fe(Al, Si)
II	65.64	2.65	…	Bal.	Fe2(Al,Si)5
III	37.32	15.37	…	Bal.	Fe(Al,Si)

Fig. 1 Microstructure of (a) base material and (b) Al-Si coating

Table 2 Chemical compositions (wt.%) and tensile properties of base materials

| | Chemical compositions (wt.%) | | | | | | | | | | Tensile properties |
	C	Mn	Si	Cr	Ti	B	Al	Fe	UTS, MPa	YS, MPa	Elongations, %
22MnB5	0.23	1.13	0.27	0.16	0.038	0.0025	0.037	Bal.	1500	1200	4.1
ER110S-G	0.1	1.2	0.6	…	…	…	…	Bal.	…	…	…
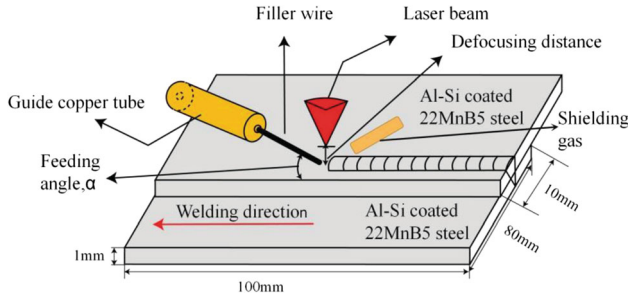
Fig. 2 Schematic setup of laser lap welding for adding filler wire
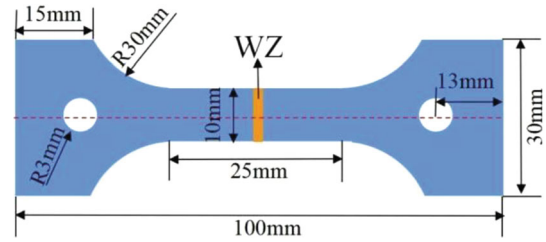

Fig. 3 Dimensions of the tensile shear testing specimen

Table 3 Welding parameters for this experiment

No.	Welding speed, m min^{-1}	Laser power, kW	Feeding speed, m min^{-1}
1	2	2.5	0
2	2	2.5	0.7
3	2	2.5	1.4
4	2	2.5	2.1

strength was obtained at a 2 mm/min pulling speed. For every parameter, more than three specimens were adopted to get the mean value. After grinding, polishing, and etching, the metallographic specimen can be investigated. The microstructure and fracture surface analysis were observed by optical microscopy (OM) or scanning electron microscopy (SEM). The chemical composition was determined by energy-dispersive spectrometry (EDS). A Micro Vickers with a 100 g load and a 10 s duration time was used to obtain the microhardness.

3. Results and Discussion

3.1 Weld Appearance and Dilution

Figure 4 shows the welds' cross section at variable feeding speed. The weld geometry (top bead width (B_1), interface width (B_2), bottom bead width (B_3) and weld reinforcement (H)) were measured from the cross section (Fig. 4). The feeding speed influenced the profile of the joint. Without filler wire (No. 1), the upper surface was slightly concave, but with filler wire, this phenomenon disappeared. When the feeding speed was low (such as No. 1, 2), a tall cup shape welded joint was obtained. B_1 and H were low, and B_2 and B_3 were large. Further increasing the feeding speed, the shape of the welded joint changed to a bowl shape, B_1 and H increased, while B_2 and B_3 decreased. In particular, when the feeding speed was increased to 2.1 m/min, an incomplete penetration weld occurred (No. 4).

Figure 5 gives schematics of the section of the welded joint for obtaining the dilution. In the laser welding process, with or without filler wire, the energy is mainly devoted to melting the base material and the filler wire. The formula is as follows:

$$E_1 = V_1\rho_1 = s_2 vt\rho_1 \tag{Eq 1}$$

$$E_2 = V_1'\rho_1 + V_2\rho_2 = s_2' vt\rho_1 + (s_1 + s_3)vt\rho_2 \tag{Eq 2}$$

where E_1 and E_2 represent the energy of the welding process without and with filler wire, respectively, V_1 is the volume of base material melted in the weld without filler wire, V_1' and V_2 are the volume of base material and filler metal melted in the weld with filler wire, respectively, s_2 is the area of base material melted in the weld without filler wire, $s_1 + s_3$ is the area of filler metal melted in the weld, s_2' is the area of base material melted with filler wire, v denotes the welding speed, t denotes the welding time, v_s denotes the feeding speed and ρ_1 ρ_2 denotes the energy density of base material and filler wire, respectively. The meaning of each parameter is as shown in Table 4.

In laser lap welding, the input energy of the welding process with or without filler wire is the same. The energy is mainly used to melt the filler wire and the base material. Based on the conservation of energy, the formula is as follows:

$$E_1 = E_2 \tag{Eq 3}$$

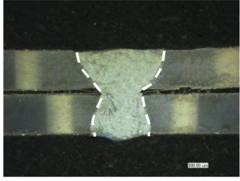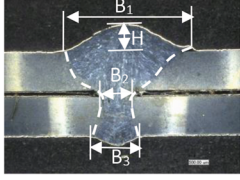$$s_2 vt\rho_1 = s_2' vt\rho_1 + (s_1 + s_3)vt\rho_2. \tag{Eq 4}$$

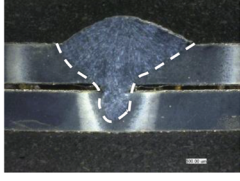| No.	Laser power (kW)	Welding speed (m·min⁻¹)	Wire feeding rate (m·min⁻¹)	H (mm)	B_1 (mm)	B_2 (mm)	B_3 (mm)	Cross-section
1	2.5	2	—	—	2.73	1.38	1.70	
2	2.5	2	0.7	0.23	2.90	1.32	1.45	
3	2.5	2	1.4	0.67	3.09	0.94	1.12	
4	2.5	2	2.1	0.79	3.74	0.82	—	

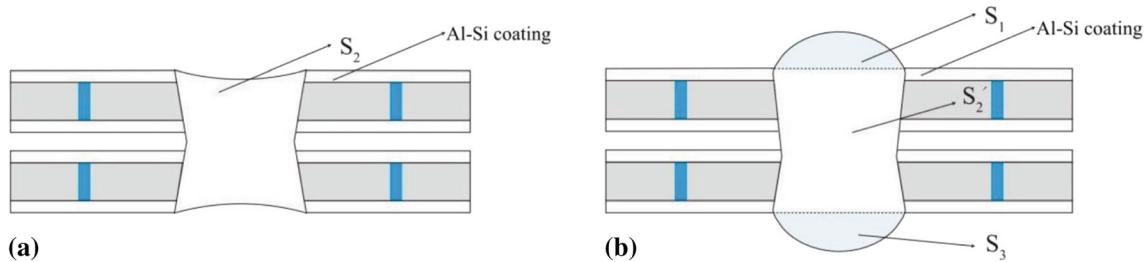**Fig. 4** Weld profile and geometry with variable welding parameters

Fig. 5 Schematics of the section of the welded joint with filler wire (a) and without filler wire (b)

The volume of the filler wire can also be expressed in terms of the feeding speed.

$$V_2 = (s_1 + s_3)vt = \pi r^2 v_s t \tag{Eq 5}$$

where r indicates the radius of the filler wire.

Bring Eq 5 into Eq 4:

$$s_2 vt\rho_1 = s_2' vt\rho_1 + \pi r^2 v_s t\rho_2. \tag{Eq 6}$$

After simplification, since only s_2 and v_s are variables:

$$s_2' = s_2 - \frac{\pi r^2 \rho_2 v_s}{v\rho_1}. \tag{Eq 7}$$

The obtained Eq 7 is very complex and difficult to understand easily by the reader. Equation 7 has been simplified to:

$$s_2' = A - Bv_s \tag{Eq 8}$$

where both A and B are constants, from Eq 8, as the feeding speed increases, the volume of the base material melted decreases $(s_2' \propto 1/)v_s)$ and from Eq 5, as the feeding speed increases, the filler wire's volume melts increases $[(s_1 + s_3) \propto v_s]$. In other words, by raising the feeding speed, more energy is absorbed by the filler wire section, which results in less energy being absorbed by the base material. That is why incomplete penetration occurred in No. 4 because the energy absorbed by the base material was inadequate to penetrate the

Table 4 The meaning of each parameter

|	
E_1	Energy of the welding process without filler wire
E_2	Energy of the welding process with filler wire
V_1	Volume of base material melted in the weld without filler wire
V_1'	Volume of base material melted in the weld with filler wire
V_2	Volume of filler wire melted in the weld with filler wire
$s_1 + s_3$	Area of filler wire melted in the weld with filler wire
s_2'	Area of base material melted in the weld with filler wire
s_2	Area of base material melted in the weld without filler wire
v	Welding speed
t	Welding time
v_s	Feeding speed
ρ_1	Energy density of base material
ρ_2	Energy density of filler wire
D	Ratio of the volume of base material in the weld to the total volume of the weld
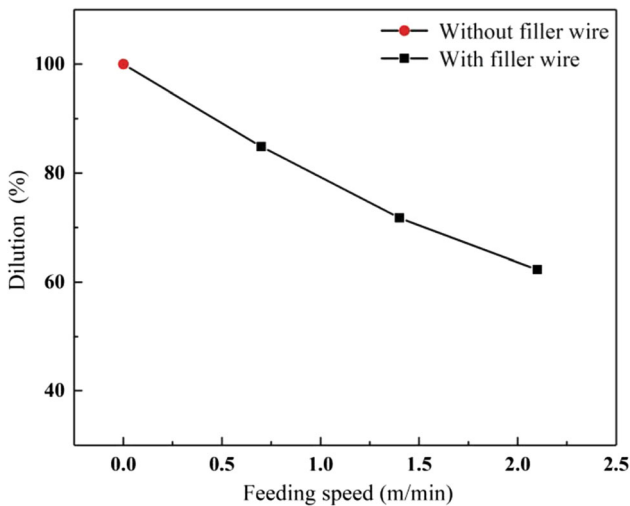
Fig. 6 Ratio of D for different feeding speeds

bottom metal. Meanwhile, more energy used to melt the filler wire led to the H and B_1 increasing. B_2 and B_3 decreased.

This dilution is defined as D. This value represents the ratio of the volume of base material in the weld to the total volume of the weld. The formula is as follows:

$$D = \frac{V_1'}{V_1' + V_2} = \frac{s_2'}{s_1 + s_2' + s_3}. \tag{Eq 9}$$

Bring Eq 5 and 8 into Eq 9. The dilution D is as follows:

$$D = \frac{B - Av_s}{\frac{\pi r^2 \times v_s}{v} + B - Av_s}. \tag{Eq 10}$$

Equation 10 is simplified to:

$$D = \frac{B - Av_s}{B - (A - C)v_s} \tag{Eq 11}$$

where C is also a constant. From equation 11, as the feeding speed increases, the value of D decreases ($D \propto 1/v_s$). As more and more filler wire enters the fusion zone, the proportion of molten base material becomes smaller and smaller. Since the volume of coating melted into the fusion zone is directly proportional to the volume of the base material melted

$(s_{coating} \propto s_2')$, the relationship between the dilution of coating and the feeding speed is the same as that between the dilution of base material and the feeding speed. The ratio of D for different feeding speeds is shown in Fig 6. With the increased feeding speed, the dilution of base material (coating) increased. That is to say, high feeding speed is good for diluting Al-Si coating and leads to the reduction of δ-ferrite in the weld.

3.2 Microstructure

Optical images of the cross-sectional microstructure and microhardness of joints with the typical parameter (No. 3) are shown in Fig. 7. The joint was divided into three zones: the fusion zone (FZ), the heat-affected zone (HAZ), and the base material (BM). The HAZ consisted of a coarse grain heat-affected zone (CGHAZ), a fine grain heat-affected zone (FGHAZ), an intercritical heat-affected zone (ICGHAZ) and a tempered zone (TZ). Fig. 8 gives their SEM images of the microstructure.

In FZ, a columnar structure was formed based on Fig. 7(b). The microscopic structure of FZ was a lath-like form, and its microhardness was high at 400-488 $HV_{0.1}$. During laser welding, the cooling speed in FZ was greater than the critical rate of martensitic transformation. Therefore, columnar austenite first solidifies and then transforms into martensite through phase transformation with shear mode. A lath-lake form was obtained as a result of low carbon content.

In HAZ, different structural features were found at different positions because of the variable thermal cycle. In CGHAZ and FGHAZ, the heating temperature exceeded the austenitic complete transition temperature A_{C3}. A complete austenitic transformation occurred first, and martensite formed in the following owing to the rapid cooling rate. However, the grain size of CGHAZ was larger than FGHAZ since the peak heating temperature in this zone exceeded the temperature (about 1100 °C) at which the grain grew seriously. In ICGHAZ, the peak heating temperature was between A_{C3} and A_{C1}. In ICGHAZ, incomplete austenitic transformation occurred, resulting in mixed structures of martensite and ferrite (as seen in Figs. 7(d) and 8(d)). In TZ, the microhardness (about 327 $HV_{0.1}$) is the lowest in HAZ. The tempered martensite formed because the peak heating temperature in TZ was below A_{C1}, as shown in Fig. 7(d) and Fig. 8(e).

In this experiment, a white band-like structure was found in all welds and it existed preferably along the fusion boundary
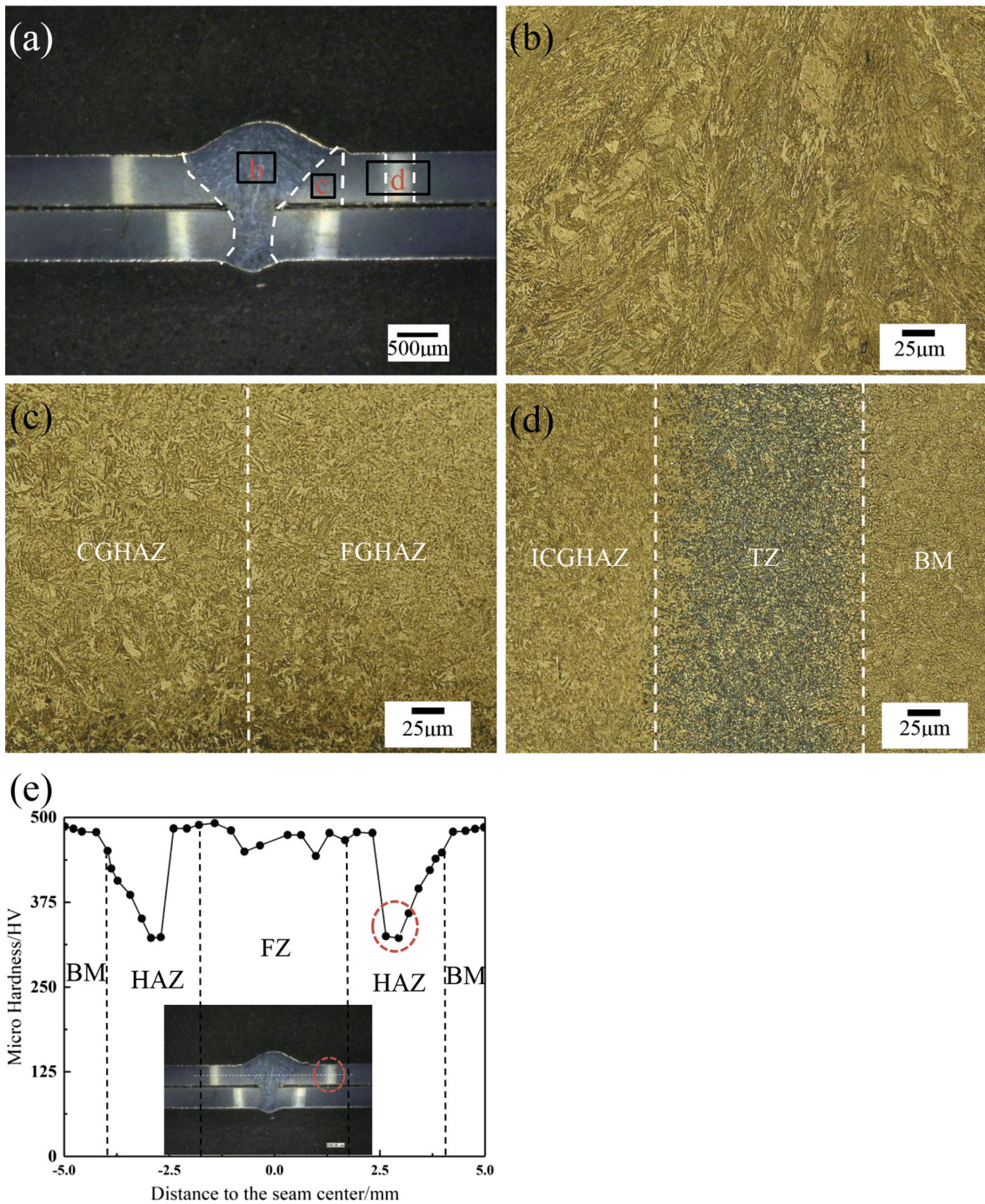
Fig. 7 Microstructures and microhardness profile of the typical weld: (a) over view; (b) fusion zone; (c) coarse grain heat-affected zone and fine grain heat-affected zone; (d) intercritical heat-affected zone and tempered zone; (e) microhardness profile

(FB). The magnified image and EDS analysis of the structure are given in Fig. 9 and Table 5, respectively. The white phase contained 3.56 wt.%Al content (P_2), which was much greater than the value for the center of the weld (P_1) (0.47 wt.%). According to the Fe-Al diagram phase, it was probably δ-ferrite which presented low strength and ductility. This is consistent with our previous study (Ref 12, 24). As a result of the existence of Al-Si on base material surfaces, the rich-Al coating melted and flew into the weld pool. It tended to accumulate along the FB owing to the quick cooling rate and flow characteristic of the weld pool.

Figure 10 indicates the white phase distribution at the FB under different feeding speeds. When combined with Fig. 9(a), the accumulation of the Al-rich phase was severe without the filler wire, and the accumulation of the Al-rich phase was gradually relieved as the feeding speed was increased. This can be explained by the schematic diagrams of weld pool flows in Fig. 11. Firstly, compared to the condition without filler wire, the dilution of Al in the upper half of the molten pool became apparent because the droplets formed and dropped into the pool, which could break the floating molten aluminum and enhance the agitation of the upper half of the pool. In addition,
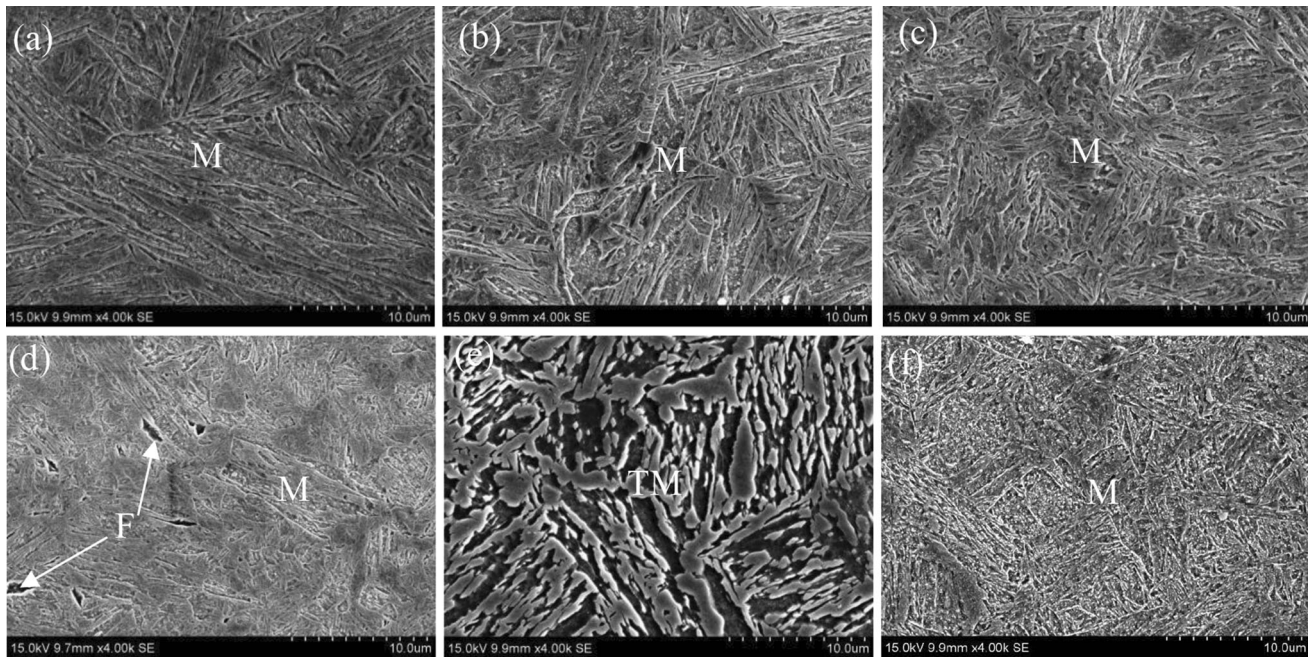
Fig. 8 SEM images of weld: (a) fusion zone; (b) coarse grain heat-affected zone; (c) fine grain heat-affected zone; (d) intercritical heat-affected zone; (e) tempered zone; (f) base material
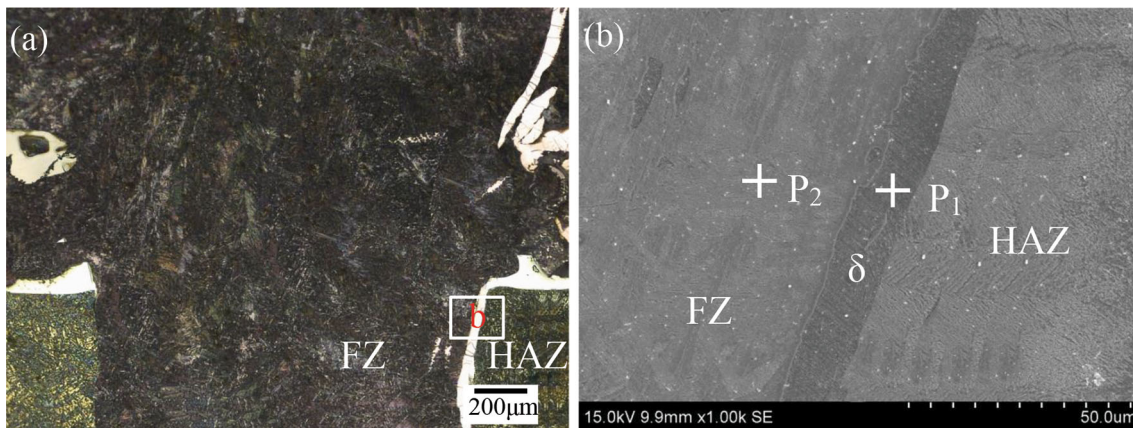

Fig. 9 Microstructure without filler metal (No. 1): (a) optical image (b) magnified SEM of FB

Table 5 Chemical compositions for different regions (wt.%)

Element/wt.%	Al	Si	Fe	Phases
P_1	3.56	0.52	Bal.	δ
P_2	0.47	0.34	Bal.	M

the defocusing distance of + 3 mm indicates that more energy was applied to the heat filler wire and the upper half of the base material. This led to the volume of the upper melt pool increasing. The dilution of aluminum in the upper half of the molten pool was enhanced. Meanwhile, less energy was used to melt the bottom half of the molten pool, which provided a shallower keyhole. Therefore, the agitation of the bottom half of the molten pool weakened, which resulted in a weaker dilution of the aluminum. In summary, the flow law of the weld

pool decided that the molten Al easily accumulated along the FB as a result of the quick cooling rate of laser welding. Consequently, a great amount of band-like δ-ferrite was found along FB. Moreover, with the increased feeding speed of the filler wire, the accumulation of Al in the upper half of the molten pool weakened while it increased in the bottom half of the molten pool.

3.3 Mechanical Properties

The average tensile shear loads and fracture locations of welded joints with different experimental parameters after tensile shear testing are shown in Table 6 and Fig. 12. Without the filler wire, the tensile shear load was very low (4355N, No. 1). With the increased feeding speed, the load increased, but when the feeding speed was increased to 2.1 m/min, the load decreased (see Fig. 13. A fracture occurred in the upper FB without filler wire. With filler wire, the fracture shifted to the
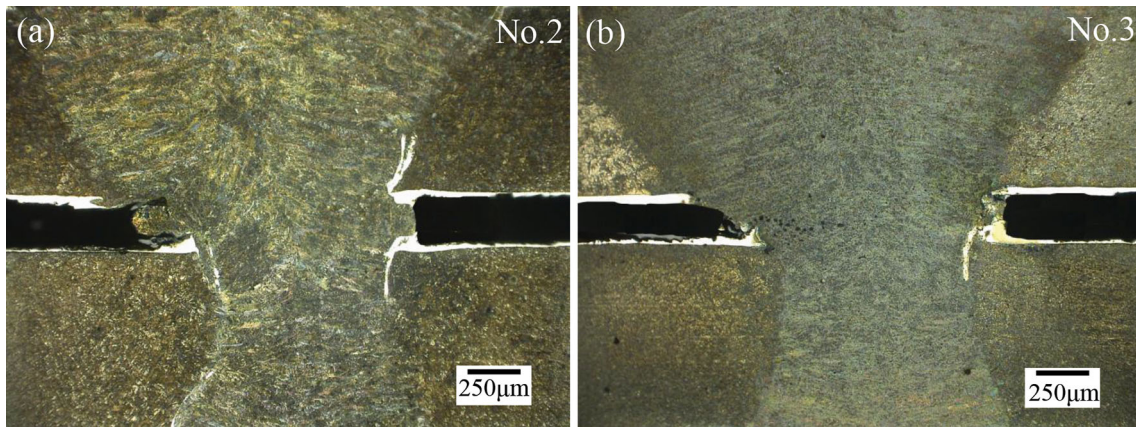
Fig. 10 Distribution of δ- ferrite under different feeding speeds (a) No. 2 (0.7 m min^{-1}); (b) No. 3 (1.4 m min^{-1})
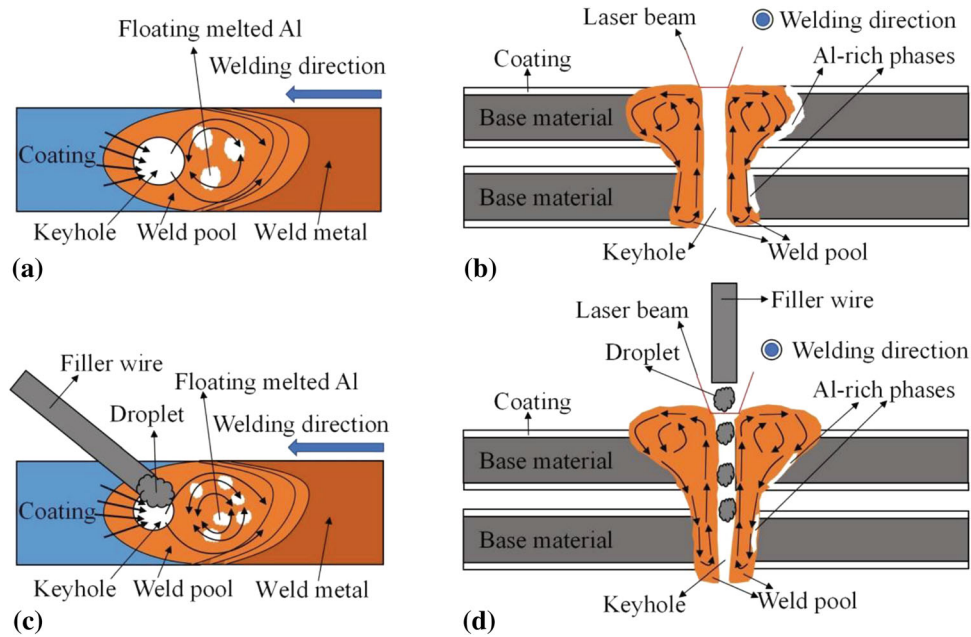

Fig. 11 Schematic diagrams of weld pool flows in laser welding: (a) top view and (b) front view without filler wire; (c) top view and (d) front view with filler wire

Table 6 Tensile shear strength and fracture location

No.	Laser power, kW	Welding speed, m min^{-1}	Feeding speed, m min^{-1}	Tensile shear load, N	Tensile shear strength, MPa	Fracture location
1	2.5	2	…	4355	436	Upper FB
2	2.5	2	0.7	5968	597	Bottom FB
3	2.5	2	1.4	7456	746	Bottom FB
4	2.5	2	2.1	5897	719	Interface

bottom FB, with the exception of No. 4, which fractured at the interface.

Figure 14 depicts the typical fracture morphology of a welded joint with (No. 3) and without (No. 1) filler wire. The fracture surfaces presented two fracture patterns. A portion of the fracture surface displayed river patterns and tear ridges, indicating a quasi-cleavage fracture pattern (Figs. 14(a) D1 and (c) D3). The other showed many dimples, which indicated a

ductile fracture pattern (Fig. 14(b) D2 and Fig. (d) D4). Consequently, the failure mode mixed quasi-cleavage and ductile fracture. Compared to two fracture surfaces, the proportion of quasi-cleavage fracture without filler wire was obviously greater than that with filler metal.

To further investigate the fracture location, the fracture surfaces were analyzed by EDS. Table 7 gives the chemical composition of different points on fracture surfaces. The
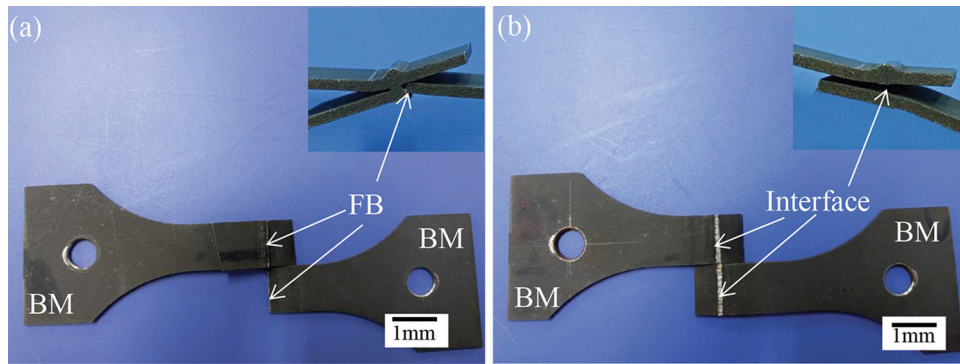
Fig. 12 Typical failure locations: (a) FB (No. 3); (b) interface (No. 4)
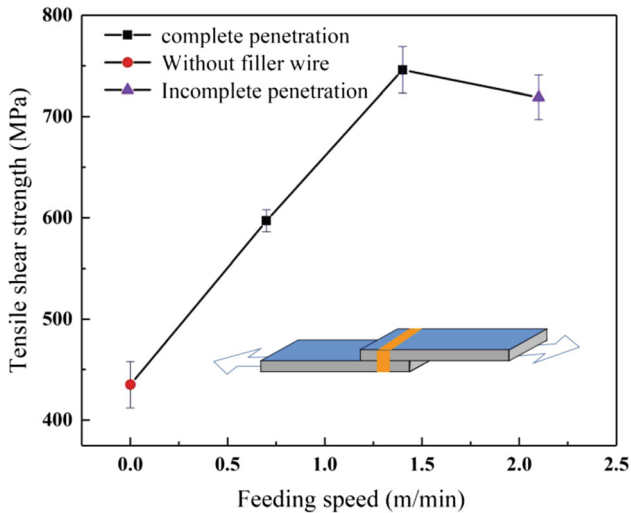

Fig. 13 Tensile shear strength with different feeding speeds

aluminum content of the cleavage planes with and without filler metal was 4.32 wt.% (D_1) and 6.83 wt.% (D_3), respectively, while the aluminum content of the dimples was 1.02 wt.% (D_2) and 1.67 wt.% (D_4), respectively. Combined with the result of the microstructure of the welded joints, the fracture exhibited quasi-cleavage fracture pattern in the δ-ferrite phases (such as D_1 and D_3) while exhibited ductile fracture pattern in the martensite phases (such as D_2 and D_4). Namely, during the welding process, the Al-Si coating melted and dissolved in the weld, forming a low-strength and ductile Al-rich phase (δ-ferrite). It was especially prevalent along the FB. Therefore, the crack easily formed and propagated in δ-ferrite along FB and then propagated to martensite. Due to it, poor strength with the Al-Si coating was obtained (Ref 24). Two fracture patterns existed in the welded joint. In addition, the higher feeding speed under filler wire conditions resulted in less dilution of Al. Consistently, the mechanical properties of the welded joints increased. However, excessive feeding rate led to lack of penetration and a very small interface area, which resulted in the interfacial fracture.

4. Conclusions

This study used a fiber laser to weld Al-Si coated 22MnB5 hot stamping steel with filler wire. The influence of the feeding speed on the microstructure and mechanical properties of welded joints was studied, and the following conclusions were drawn:

(1) The feeding speed influenced the weld shape and dilution of the coating. Raising the feeding speed, the weld changed from a tall cup shape to a bowl shape $\left[s_2' \alpha 1/v_s \text{ and } (s_1 + s_3) \alpha v_s\right]$. The dilution of coating decreased $s_{\text{coating}} \propto s_2'$ and $\propto 1/$ and $D \propto 1 v_s$.

(2) Because of the rapid cooling rate during laser welding, the microstructure of the fusion zone was lath-like martensite. As a result of thermal conductivity, the heat-affected zone (HAZ) could be divided into three types: coarse grain heat-affected zone (CGHAZ) (whose microstructure was coarse martensite), fine grain heat-affected zone (FGHAZ) (whose microstructure was fine martensite), intercritical heat-affected zone (ICGHAZ) (whose microstructure was ferrite and martensite) and a tempered zone (TZ) (whose microstructure was tempered martensite with the lowest hardness). Al-Si melted into the fusion zone and formed δ-ferrite at FB. The accumulation of δ-ferrite at FB decreased as the feeding speed of the filler wire increased.

(3) The maximum tensile shear strength of joints was 746 MPa, which was more than that without filler wire condition (436 MPa). Except for the high feeding speed of the filler wire, the failure occurred in the FB, which exhibited a mixture failure mode of quasi-cleavage and dimple fracture.
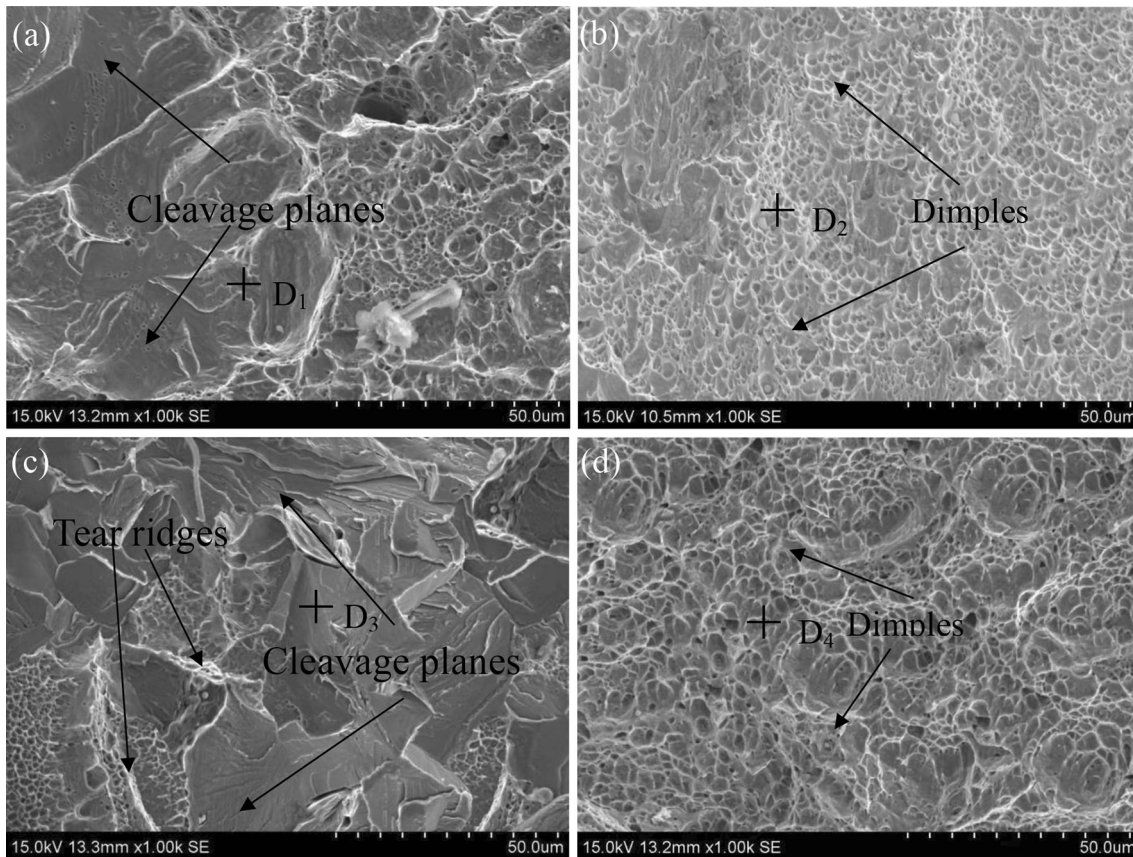
Fig. 14 SEM morphologies of fracture surfaces with filler wire (a, b) and without filler wire (c, d)

Table 7 Chemical compositions of fracture surfaces (wt.%)

Element/wt.%	D_1	D_2	D_3	D_4
Al	4.32	1.02	6.83	1.67
Si	0.56	0.35	0.93	0.72
Fe	Bal.	Bal.	Bal.	Bal.

References

1. M. Pfestorf, Manufacturing of High Strength Steel and Aluminum for a Mixed Material Body in White, *J. Adv. Mater. Res.*, 2005, **6–8**, p 109–126

2. H. Samuel, K. Jörgen, L. Simon and J.P. Jonsén, Ultra High Strength Steel Sandwich for Lightweight Applications, *SN. Appl. Sci*, 2020, **2**, p 1040–1055

3. J.H. Schmitt and T. Iung, New Developments of Advanced High-Strength Steels for Automotive Applications, *C. R. Phys*, 2018, **19**, p 641–656

4. H. Karbasian and A.E. Tekkaya, A Review on Hot Stamping, *J. Mater. Process. Technol*, 2010, **210**, p 2103–2118

5. K. Mori and D. Ito, Prevention of Oxidation in hot Stamping of Quenchable Steel Sheet by Oxidation Preventive Oil, *CIRP. Ann. Manuf. Technol.*, 2009, **58**, p 267–270

6. O.L. Ighodaro, E. Biro and Y.N. Zhou, Comparative Effects of Al-Si and Galvannealed Coatings on the Properties of Resistance Spot Welded hot Stamping Steel Joints, *J. Mater. Process. Technol.*, 2016, **236**, p 64–72

7. D.W. Zhou, S.H. Xu, L. Peng and J.S. Liu, Laser lap Welding Quality of Steel/Aluminum Dissimilar Metal Joint and its Electronic Simulations, *Int. J. Adv. Manuf. Technol.*, 2016, **86**, p 2231–2242

8. S.H. Chen, J.H. Huang, K. Ma, H. Zhang and X.K. Zhao, Influence of a Ni-foil Interlayer on Fe/Al Dissimilar Joint by Laser Penetration Welding, *Mater. Lett.*, 2012, **79**, p 296–299

9. J.H. Sun, Q. Yan, W. Gao and J. Huang, Investigation of Laser Welding on butt Joints of Al/steel Dissimilar Materials, *Mater. Des.*, 2015, **83**, p 120–128

10. K.J. Lee, S. Kumai, N. Kawamura, N. Ishikawa and K. Furuya, Growth Manner of Intermetallic Compounds at the Weld Interface of Steel/Aluminum Alloy Lap Joint Fabricated by a Defocused Laser Beam, *Mater. Trans.*, 2007, **48**, p 1396–1405

11. J. Jia, S.L. Yang, W.Y. Ni and J.Y. Bai, Microstructure and Mechanical Properties of fiber Laser Welded Joints of Ultrahigh-Strength Steel 22MnB5 and Dual-Phase Steels, *J. Mater. Res.*, 2014, **29**, p 2565–2575

12. X. He, Y.Q. Qin and W.X. Jiang, Effect of Welding Parameters on Microstructure and Mechanical Properties of Laser Welded Al-Si Coated 22MnB5 hot Stamping Steel, *J. Mater. Process. Technol.*, 2019, **270**, p 285–290

13. B. Gerhards, U. Reisgen and S. Olschok, Laser Welding of Ultrahigh Strength Steels at Subzero Temperatures, *Phys. Proced.*, 2016, **83**, p 352–361

14. Y.L. Li, Y.R. Liu and J. Yang, First Principle Calculations and Mechanical Properties of the Intermetallic Compounds in a Laser Welded Steel/Aluminum Joint, *Opt. Laser Technol.*, 2020, **122**, p 105875

15. M. Kang, C. Kim and J. Lee, Weld Strength of Laser-Welded hot-Press-Forming Steel, *J. Laser Appl.*, 2012, **24**, p 208–219

16. C. Kim, M.J. Kang and Y.D. Park, Laser Welding of Al-Si Coated hot Stamping Steel, *Pro. Eng.*, 2011, **10**, p 2226–2231

17. W.H. Lin, F. Li, D.S. Wu, X.G. Chen, X.M. Hua and H. Pan, Effect of Al-Si Coating on Weld Microstructure and Properties of 22MnB5 Steel Joints for hot Stamping, *J. Mater. Eng. Perform.*, 2017, **27**, p 1825–1836

18. D.C. Saha, E. Biro, A.P. Gerlich and Y.N. Zhou, Fiber Laser Welding of Al-Si Coated Press-Hardened Steel, *Weld. J.*, 2016, **95**, p 147s–156s

19. M.S. Khan, M.H. Razmpoosh, A. Macwan, E. Biro and Y. Zhou, Optimizing Weld Morphology and Mechanical Properties of Laser Welded Al-Si Coated 22MnB5 by Surface Application of Colloidal Graphite, *J. Mater. Process. Tech.*, 2021, **293**, p 117093

20. X.N. Wang, X.M. Chen, Q. Sun, H.S. Di and L.N. Sun, Formation Mechanism of δ-Ferrite and Metallurgy Reaction in Molten Pool During Press-Hardened Steel Laser Welding, *Mater. Lett.*, 2017, **206**, p 143–145

21. T.Flehmig, D. Scheuvens, L. Homig, *Device and method for partial decoating and/or machining of material from a workpiece*, US20150239053A1, (2015)

22. S.L. Min, J.H. Moon and C.G. Kang, Investigation of Formability and Surface Micro-Crack in hot Deep Drawing by Using Laser-Welded Blank of Al-Si and Zn-Coated Boron Steel, *J. Eng. Manuf.*, 2014, **228**, p 540–552

23. H. Kügler, C. Mittelstädt and F. Vollertsen, Influence of Joint Configuration on the Strength of Laser Welded Presshardened Steel, *J. Phys. Proced.*, 2016, **83**, p 373–382

24. D.F. Zhang, Y.Q. Qin, F. Zhao and M. Liang, Microstructure and Mechanical Properties of Laser Welded Al-Si Coated 22MnB5 hot Stamping Steel and Galvanized Steel, *J. Mater. Eng. Perform.*, 2021, **31**, p 1346

25. W.H. Lin, F. Li, X. Hua and D. Wu, Effect of Filler Wire on Laser Welded Blanks of Al-Si-Coated 22MnB5 Steel, *J. Mater. Process. Technol.*, 2018, **259**, p 195–205